

Hysteresis Motor Using Heat Treated Fe-Cr-Ni-Mo-C Steel Alloy

Hysteresis motors are exciter less synchronous machines, which have found wide applications in sub fractional horse power ratings. These motors have some favorite features such as constant torque, low startup current and noiseless operation. However, low efficiency and low power factor are common deficiencies of the hysteresis motors, which should be rectified using more suitable rotor substance and having accuracy in design considerations as possible. In general, magnetic property of the rotor material has the most important and plays a key role in the hysteresis motors performance. In this paper, electromagnetic characteristics of a steel alloy which contains iron, chrome, nickel, molybdenum, and carbon (Fe-Cr-Ni-Mo-C) are presented and application of this steel alloy for rotor of hysteresis motors is investigated. Magnetic properties of Fe-Cr-Ni-Mo-C are compared with other common magnetic materials, used in the conventional hysteresis motors. The results confirm eligibility of Fe-Cr-Ni-Mo-C rather than others.

Keywords: Chrome, Fe-Cr-Ni-Mo-C, Hysteresis material, Hysteresis motor, Iron, Molybdenum, Nickel, Steel alloy.

Article history: Received 21 August 2014, Received in revised form 17 September 2014, Accepted 2 December 2014

Nomenclature:

Symbol	Quantity
m	Number of phases
f	Frequency
ϕ	Electrical angle
Φ_0	A constant electrical angle
Φ_m	Mechanical angle
p	Number of pole pairs
Z	The maximum value of the conductor density
K	Ratio of radii
K_w	Winding factor
N_{ph}	Number of winding turns per phase
μ	Permeability of the material
α	Hysteresis delay angle
V_r	Volume of hysteresis material
E_h	Area of the hysteresis loop
g	Air gap length
$H_g(\phi)$	Magnetic field intensity in the air gap
$H_r(\phi)$	Magnetic field intensity in the rotor
B_m	Peak values of the field density of rotor
B_s	Magnetic field density in the stator
B_g	Flux density in the air gap
B_r	Flux density in the rotor
r_l	Stator winding resistance
X_l	Stator leakage reactance
R_c	Stator iron and parasitic losses resistance
X_g	Magnetizing reactance
$R_h + jX_h$	Rotor impedance

* Corresponding author: T. Ghanbari, School of Advanced Technologies, Shiraz University, Shiraz, Iran. E-mail: ghanbarih@shirazu.ac.ir

¹ T. Ghanbari, Assistant professor, School of Advanced Technologies, Shiraz University, Shiraz, Iran.

² Faculty of Electrical and Robotics Engineering, Shahrood University of Technology, Shahrood, Iran

1. Introduction

Hysteresis motors are self starting brushless synchronous motors which is the best option for some particular applications due to a few unique specifications. Fig. 1 shows a simple structure of a conventional cylindrical hysteresis motor. Stator of the hysteresis motors are wounded like as conventional motors, while the rotor is only a solid ring made from a hysteresis material. Although hysteresis motors have low efficiency and low power factor, these motors are widely used in navigation and military apparatus due to some attractive and outstanding features (1)-(4). Different structures of hysteresis motors are presented, which each of them have some outstanding specifications for one or more applications (5), (6). In order to have the best possible performance for the hysteresis motors, having an accurate model for the machine is necessary (7)-(11).

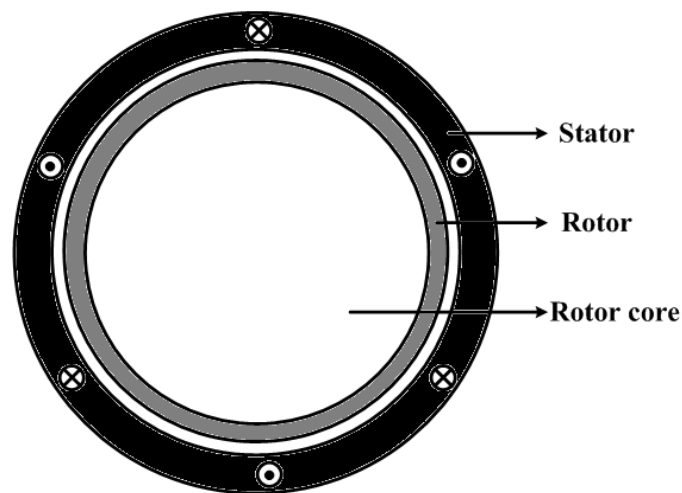


Fig. 1. Simple structure of a cylindrical hysteresis motor

Selection of the rotor hysteresis material with desirable magnetic characteristic is the most important key point for having a high performance hysteresis motor. A few hysteresis materials such as 36% Cobalt steel (Fe-36% Cobalt), Alnico (Fe-Co-Ni-Al) and Chrome cobalt steel (Fe-Cr-Co) are suggested to utilize in rotor of hysteresis motors (12)-(17). In this paper, it is confirmed that Fe-Cr-Ni-Mo-C steel alloy could be a good alternative option for rotor of hysteresis motor due to its suitable magnetic specifications. The magnetic characteristics of Fe-Cr-Ni-Mo-C alloy are measured and compared to corresponding characteristics of 36% Cobalt steel (Fe-36% Cobalt), Alnico (Fe-Co-Ni-Al) and Chrome cobalt steel (Fe-Cr-Co). Different materials impact on the motor performance is analyzed and the advantages of Fe-Cr-Ni-Mo-C are presented.

2. Modeling

The following assumptions are considered to simplify the analysis:

- a) The motor rotates by maximum load in synchronism condition.
- b) The stator has sinusoidal distribution poly-phase windings and its magnetic motive force (mmf) is produced by sinusoidal currents. The resultant fundamental component of the magnetic motive force in the steady state condition can be calculated by:

$$F = \frac{3}{2} \sqrt{2} I Z \cos(\omega t - \phi) \quad (1)$$

in which:

$$Z = \frac{2K_w N_{ph}}{p\pi} \quad (2)$$

c) In the reference (4) the hysteresis loops are approximated by parallelograms and in the references (18) and (19) they are estimated by ellipses, with two variables μ and α . More accurate modeling approaches of the hysteresis loops have been presented in (20) and (21). However, fundamental components of the flux density and field intensity of the rotor for a given operation condition can be written as follow:

$$B = B_m \cos(\omega t - \phi - \phi_0) \quad (3)$$

$$H = H_m \cos(\omega t - \phi - \phi_0 + \alpha) \quad (4)$$

in which:

$$H_m = \frac{B_m}{\mu} \quad (5)$$

$$\alpha = \sin^{-1} \left(\frac{E_h}{\pi H_m B_m} \right) \quad (6)$$

e) The thickness of the rotor is sufficiently small, so the flux density of the ring only consists of circumferential components.

Using Ampere's circuital law in a closed path including rotor and stator as shown in Fig.2 gives:

$$H_g(\phi)g + H_r(\phi)r \frac{d\phi}{p} - (H_g(\phi) + dH_g(\phi))g = F d\phi \quad (7)$$

in which:

$$F = \frac{r}{p} H_r(\phi) - g \frac{dH_g(\phi)}{d\phi} \quad (8)$$

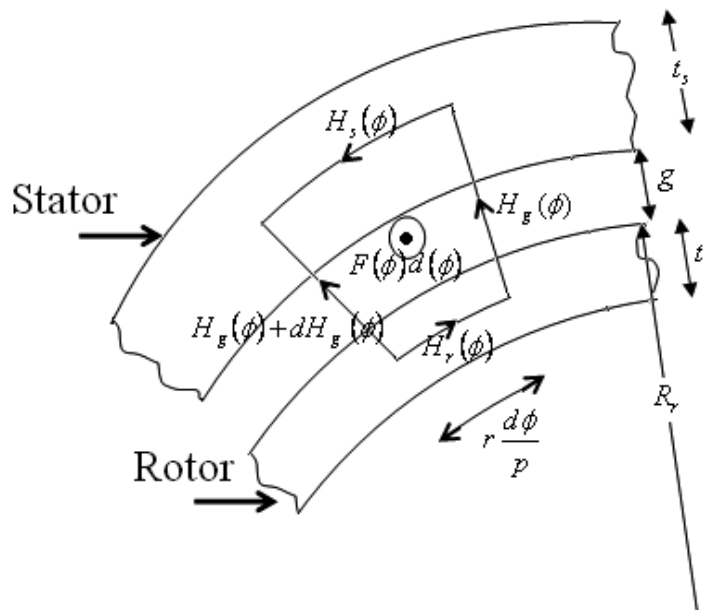


Fig. 2. A closed path including rotor and stator

According to Fig. 3, applying the continuity principle will give the flux density of the air gap. If magnetic field intensity in rotor is defined by:

$$H_r(\phi) = \frac{B_m}{\mu} \cos(\omega t - \phi - \phi_0 + \alpha) \quad (9)$$

So:

$$l t_r (B_r(\phi) + dB_r(\phi)) - l t_r B_r(\phi) = B_g(\phi) l (R_r + g) \frac{d\phi}{p} \quad (10)$$

$$B_g(\phi) = \frac{p t_r dB_r(\phi)}{(R_r + g) d\phi} \quad (11)$$

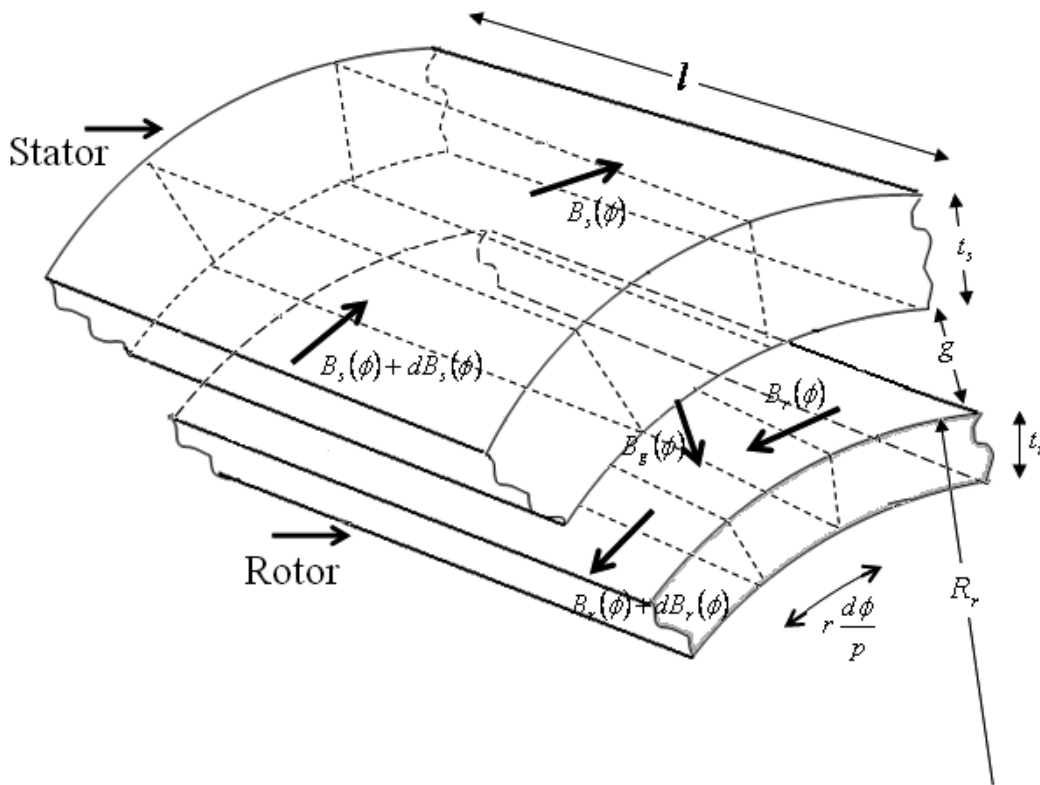


Fig. 3. Flux in the infinitesimal angle ($d\phi$) of rotor, stator and air gaps

In equations (11), $B_g(\phi)$ is the space dependent flux density of the air gap and $B_r(\phi) = B_m \cos(\omega t - \phi - \phi_0)$ is the flux density of the rotor.

In stator we have:

$$l t_s (B_s(\phi) + dB_s(\phi)) - l t_s B_s(\phi) = B_g(\phi) (R_r + g) \frac{d\phi}{p} \quad (12)$$

$$\frac{dB_s(\phi)}{d\phi} = \frac{(R_r + g) B_g(\phi)}{l t_r} \quad (13)$$

From equations (11) and (13) one can derive:

$$\frac{dB_s(\phi)}{d\phi} = p \frac{dB_r(\phi)}{d\phi} \quad (14)$$

Using this equation one can calculate stator flux density and core losses.

Combination of equations (7)-(13) gives:

$$\frac{3}{2} \sqrt{2} I Z \cos(\omega t - \phi) = \frac{R_{av} B_m}{p\mu} \cos(\omega t - \phi - \phi_0 + \alpha) + \frac{gp t_r B_m}{(R_r + g)} \cos(\omega t - \phi - \phi_0) \quad (15)$$

To obtain an equivalent circuit for the hysteresis motor, first the induced voltage of each phase of the stator winding is calculated and the phase current is divided to different components. For calculation of the induced voltage, linkage flux of one turn winding including two conductors located in positions ϕ and $\phi + \pi$, is calculated by:

$$\varphi = l(R_r + g) \int_{\phi}^{\phi+\pi} B_g(\phi) \frac{d\phi}{p} \quad (16)$$

Substitution equation (11) in (16):

$$\varphi = l t_r \cos(\omega t - \phi - \phi_0) \quad (17)$$

Therefore, the induced voltage in one conductor located in the position ϕ will be:

$0.5 \left(\frac{d\varphi}{dt} \right)$, so, the induced voltage in phase a will be:

$$e_a = \int_0^{2p\pi} \frac{1}{2} \left(\frac{d\varphi}{dt} \right) Z \cos(\phi) d\phi \quad (18)$$

$$e_a = \omega K_w N_{ph} l t_r \cos(\omega t - \phi_0 + \frac{\pi}{2}) \quad (19)$$

Now, by dividing both sides of equation (15) on $1.5Z$ and setting the value of $\phi = (n-1) * 1.5\pi$ (for phase a the value of n is one), gives:

$$\sqrt{2} I \cos(\omega t - \phi) = \frac{\pi R_{av} B_m}{3 K_w N_{ph} \mu} \cos(\omega t - \phi - \phi_0 + \alpha) + \frac{\pi g p^2 t_r B_m}{3 K_w N_{ph} (R_r + g)} \cos(\omega t - \phi - \phi_0) \quad (20)$$

In the left side of equation (20), the current of phase a with phase angle $0.5\pi - \phi_0$ regarding the induced voltage of phase a appears. In the other side of this equation, two components of the phase current with different phase angles come out.

$$i_a = i_h + i_g \quad (21)$$

Therefore, the calculated air gap or magnetizing reactances and impedances of the rotor seen by the stator side will be respectively as:

$$j X_{g1} = j \frac{3\omega K_w N_{ph} l t_r \mu_0 (R_r + g) Z}{2gp t_r B_m} \quad (22)$$

$$Z_h = R_h + jX_h = \frac{3\omega K_w N_{ph} l t_r p \mu Z}{2R_{av} B_m} \angle \frac{\pi}{2} - \alpha \quad (23)$$

Consequently, an equivalent circuit for the hysteresis motor is obtained as shown in Fig. 4, in which its elements are introduced in the nomenclature.

As mentioned earlier the output power and hysteresis torque are related to the area of hysteresis loop, can be calculated by:

$$P_{hs} = E_h f_s V_r \quad (24)$$

$$T_{hs} = \frac{E_h V_r p}{4\pi} \quad (25)$$

3. Selection of the appropriate material for hysteresis motor

Performance of a hysteresis motor strictly depends on the rotor ring material and the rotor material is chosen considering the following key points:

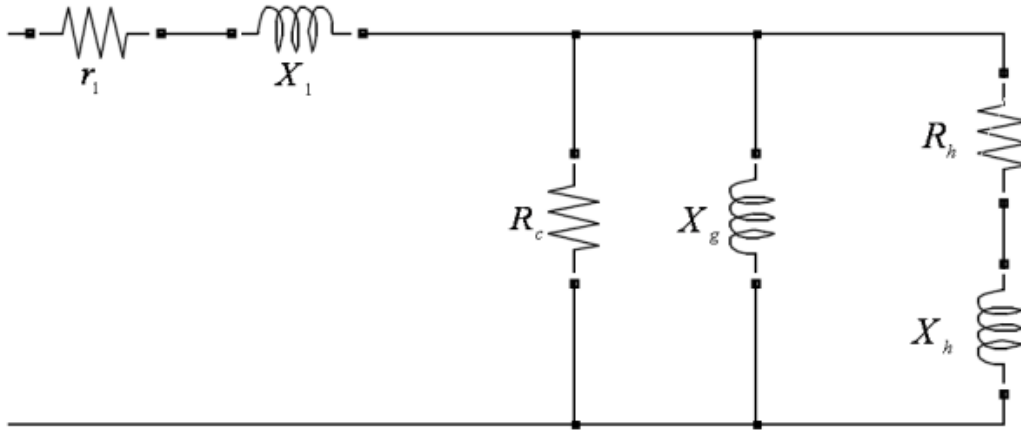


Fig. 4. Steady state equivalent circuit per phase of hysteresis motor

1- The output power of hysteresis motor depends on the area of hysteresis loop and volume of the rotor ring proportionally. Therefore, higher output power density can be realized for a wider area hysteresis loops.

2- The stator magnetizing current and in consequence copper loss will be low if the magnetic field intensity of the hysteresis loop is small and the permeability of the loop is high. Therefore, the maximum efficiency is achieved, when the machine works on one of the hysteresis loops called normal loop.

3- Higher output torques are achieved in more hysteresis delay angles for a hysteresis motor.

4- Minor loops and corresponding parasitic losses of the rotor rings are produced by MMF harmonic content including slotting effects (22), (23). It is known that slope of minor loops is equal to the slope of the magnetizing curve at the maximum point of relevant hysteresis loop. A hysteresis loop and a few minor loops are shown in Fig. 5. The parasitic losses have a reverse relation with the minor loops slope. Therefore, one of the important factors in selection of the rotor material is the value of magnetizing curve slope at the maximum point of the normal loop.

5- In the hysteresis motors, the torque corresponding to the eddy current is added to the hysteresis torque during startup (1). Eddy current torque depends on the conductivity and volume of rotor material, area of hysteresis loop and some design parameters. Hence, the startup torque in the hysteresis motor can be improved by selection of an appropriate material with higher conductivity.

6- Generally a particular heat treatment and hardening process are performed on the hysteresis materials. Therefore the hysteresis materials are mechanically hard and cause some problems for manufacturing. This matter should be taken into account, when the hysteresis material is chosen.

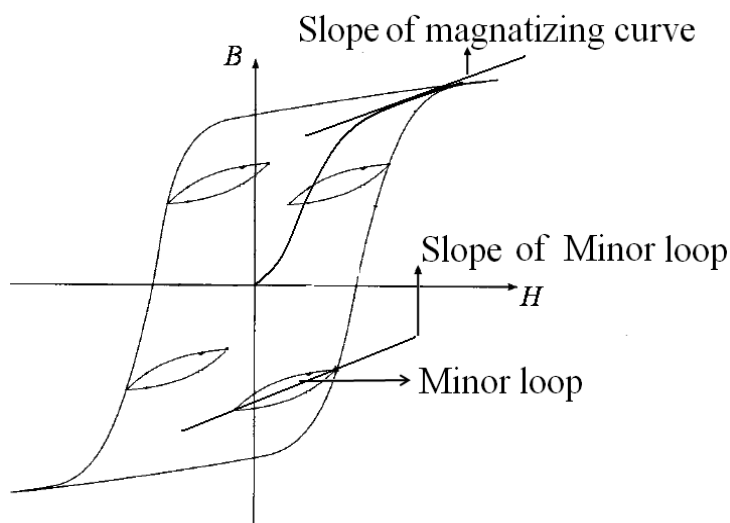


Fig. 5. A hysteresis loop and a few minor loops

5. Comparison of magnetic properties of hysteresis materials

Comparisons of magnetic characteristics for Fe-36% Cobalt, Alnico, Fe-Cr-Co and Fe-Cr-Ni-Mo-C help us to choose the best material for the hysteresis motor in different applications.

Magnetizing curves of Fe-36% Cobalt, Alnico, Fe-Cr-Co and Fe-Cr-Ni-Mo-C alloys are shown in Fig. 6. Points highlighted by "*" on the graphs in Fig. 6, represent the peak values of magnetic field intensities and flux densities of the normal loops for the materials. It can be clearly observed that Fe-Cr-Ni-Mo-C alloy goes to saturation faster than the other alloys and magnetic field intensity of the normal loop of Fe-Cr-Ni-Mo-C alloy is lower than the other alloys.

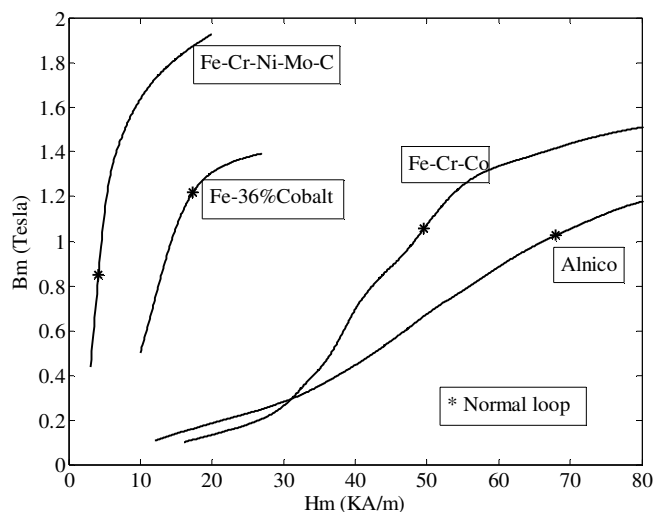


Fig. 6. Magnetizing curves and peak values of normal loops for various hysteresis materials

In addition, the magnetizing curve slope for the normal loop of Fe-Cr-Ni-Mo-C alloy is higher than the slopes for magnetizing curves of other alloys.

Relative permeability μ/μ_0 versus peak values of magnetic field intensities for various materials are shown in Fig. 7. It is evident that the relative permeability for the normal loop of Fe-Cr-Ni-Mo-C alloy is much higher than other hysteresis materials.

Since the peak value of magnetic field intensity for the normal loop of Fe-Cr-Ni-Mo-C alloy is lower than the corresponding values of the other alloys and the relative permeability for the normal loop of this alloy is higher than the others, the magnetizing current and resultant copper loss of the motor with Fe-Cr-Ni-Mo-C alloy in its rotor will be lower. Consequently, the power factor for this motor will be higher. Moreover, due to higher magnetizing curve slope for the rotor made by Fe-Cr-Ni-Mo-C alloy, the parasitic losses will be lower.

In Fig.8 hysteresis delay angle versus magnetic field density in some hysteresis materials are shown. By observing the graphs, it is clear that hysteresis delay angle of Fe-Cr-Ni-Mo-C alloy is higher than the other alloys, which causes higher generated torque. Hysteresis loops areas versus flux densities of the hysteresis materials are shown in Fig. 9.

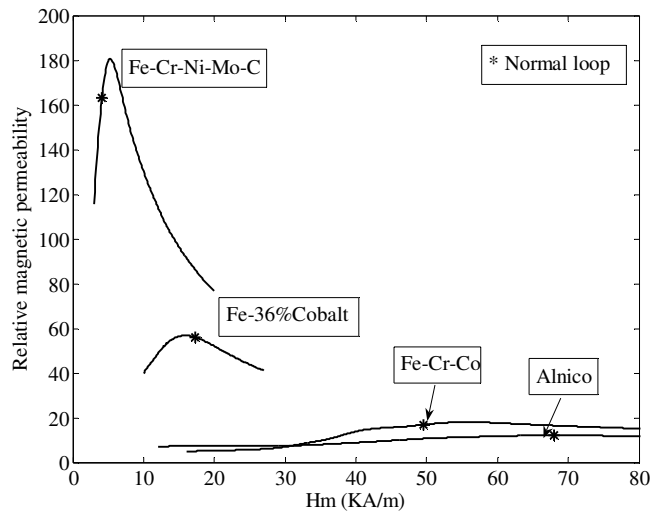


Fig. 7. Relative permeabilities versus peak values of magnetic field intensities of various hysteresis materials

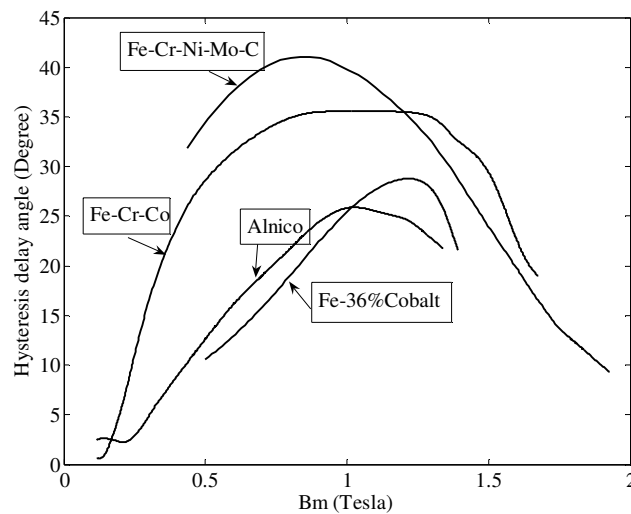


Fig. 8. Hysteresis delay angles versus peak values of flux densities of hysteresis materials

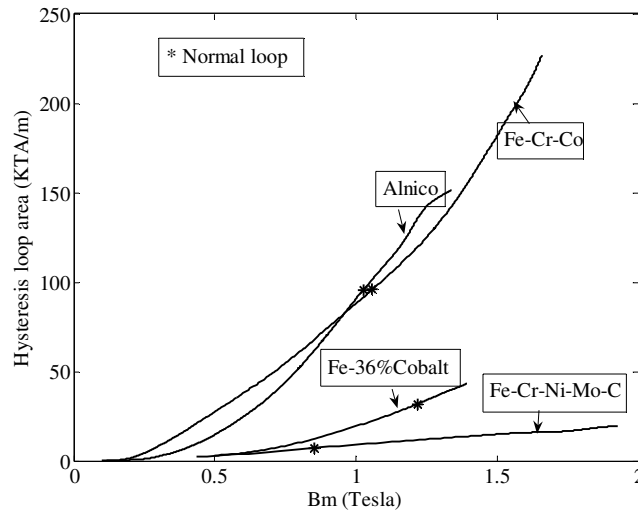


Fig. 9. Area of hysteresis loops versus peak values of flux densities for various hysteresis materials

From equation (4) one can conclude that the output power of a hysteresis motor depends on the area of hysteresis loop and volume of the rotor ring proportionally. For a given output power, due to less area of the hysteresis loop, greater hysteresis material volume is required for the hysteresis motor, in which Fe-Cr-Ni-Mo-C alloy is utilized.

Of course, increased volume and weight is not a disadvantage for some applications particularly for the apparatus, in which high moment inertia is required.

6. Simulation and experimental results

Based on the equivalent circuit shown in Fig. 4, one can straightforwardly calculate efficiency and power factor for the hysteresis motor with different rotor materials. In fact, using the information presented in figures 6-9 for different materials the rotor parameters are calculated by Eq. (22) and (23). Then, using the calculated equivalent circuit and Eq. (24) the power factors and efficiencies are computed. Calculated efficiencies and power factors of a motor with different rotor materials are shown in Fig.10. As Shown in Fig.10, efficiency and power factor of the motor with Fe-Cr-Ni-Mo-C alloy are remarkable especially in the high frequencies, whereas the volume of the rotor material as shown in Fig. 11 for 50 Hz is greater than the other materials. Although, more volume of the rotor material may be a deficiency in some applications, in some other applications such as gyroscopes it is advantageous for achieving higher rotor inertia. In all the presented simulations, the mechanical losses are ignored. Some essential design and measured parameters for a prototype motor are listed in Table 1 and the photographs of the machine and its rotor are given in Fig.12.

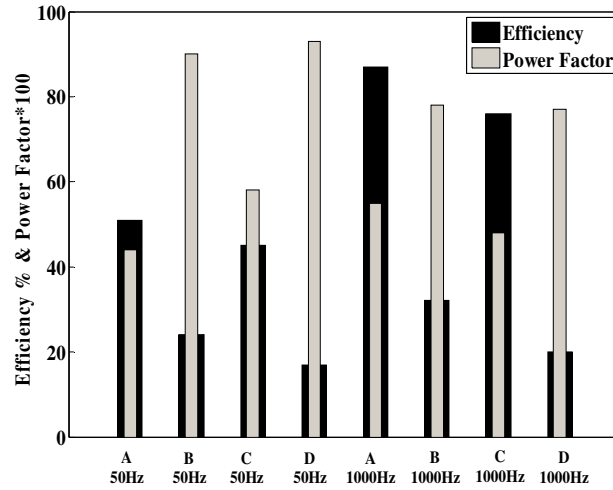


Fig. 10. Efficiencies and power factors with: A: Fe-Cr-Ni-Mo-C B: Fe-Cr-Co C: Fe - 36%Co D: Alnico

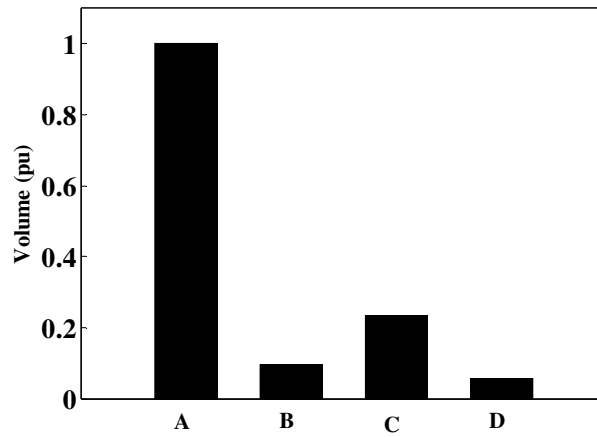


Fig. 11. Volumes of rotor materials with: A: Fe-Cr-Ni-Mo-C B: Fe-Cr-Co C: Fe-36%Co D: Alnico (for 50 Hz)

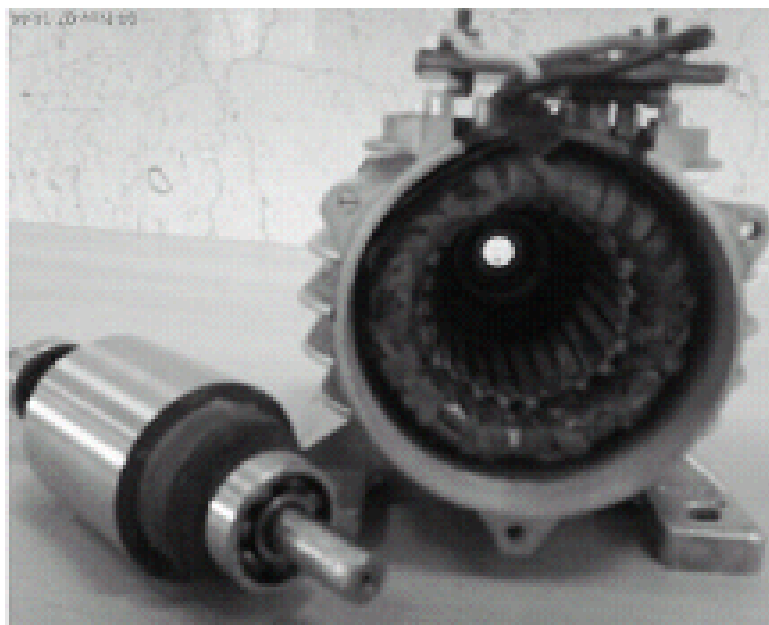


Fig. 12. The prototype fabricated motor

TABLE I

Characteristics of the motor by Fe-Cr-Ni-Mo-C alloy and some measured parameters

Symbol	Quantity	value
f	Frequency	50 Hz
V_l	Line voltage	50 V
P_{out}	Output power	25 W
PF	Power factor	0.4
I_{in}	Phase input current	1.5 A
$\eta\%$	Efficiency percent	47
T_{out}	Output torque	1 Kg.cm
m	Number of phases	3
p	Number of pole pairs	2
g	Air gap length	0.2 mm
Z	Number of stator slots	16
R_{av}	Ring mean radius	30 mm
r_r	Ring thickness	4 mm
V	Ring volume	5.3e4 mm ³
N	Number of turns/coil	32
N_c	Number of coils	95
K_w	Winding factor	0.85
l	Axial length	70 mm

7. Conclusion

In this paper magnetic characteristics of a steel alloy with composition iron, chrome, nickel, molybdenum (Fe-Cr-Ni-Mo-C) for application in rotors of hysteresis motors are presented. These properties are compared with a few materials, which are commonly employed for the rotors of the hysteresis motors. This comparison shows that utilizing this alloy with a proper design can increase the efficiency and power factor of the hysteresis motor. Even though the power density of the suggested material is lower than the other materials, it could be suitable at least in specific application such as gyroscope in which higher moment inertia of the rotor is an advantageous. Moreover, other hysteresis materials contain rare-earths and costly components such as Cobalt, but Fe-Cr-Ni-Mo-C alloy steel is cheap and available steel, so this alloy can be recommended for using in the hysteresis machines with some confidences.

References

- [1] M. A. Rahman and A M. Osheiba, Dynamic performance prediction of polyphase hysteresis motors, *IEEE Trans On Ind. App*, 26(6), 1026-1033, Nove /Dece. 1990.
- [2] M. A. Rahman and R. Qin, A permanent magnet hysteresis hybrid synchronous motor for electrical vehicles, *IEEE Trans. On Ind. Elec.*, 44(1), 44-53, 1997.
- [3] K. R. Rajagopal, Design of a Compact Hysteresis Motor Used in a Gyroscope, *IEEE Trans. On Magnetics*, 39(5), 3013-3015, 2003.
- [4] M. A. Copeland and G. R. Slemon, An analysis of the hysteresis motor: I-Analysis of the idealized machine, *IEEE Trans. Power App. Syst.*, PAS-82, 34-42, Apr. 1963.
- [5] A. Darabi, T. Ganbari and M.Sanati-Moghadam, Slotless axial flux hysteresis motor, modeling and performance calculation, *IET Electr. Power Appl.*, 3(5), 491-501, 2009.
- [6] A. Darabi, M.Sanati-Moghadam and T. Ganbari, Coreless Dual-rotor Disc Hysteresis motor, modeling and performance prediction, *Electric Power Components and Systems*, 38:5, 575-591, 2010.
- [7] A. Darabi, T. Ganbari, M. Rafiei, H. Lesani and M.Sanati-Moghadam , Dynamic performance analysis of hysteresis motor by a linear time-varying model, *Iranian Journal of Electrical and Electronic Engineering*,

- 4(4), 202-215, 2008.
- [8] M. Reddy, L.V. Suresh, Dynamic analysis of hysteresis motor using Matlab/simulink, *International Journal of Engineering Research & Technology*, 1(5), 1-8, 2012.
 - [9] M. Repetto, P. Uzunov, Analysis of hysteresis motor starting torque using finite element method and scalar static hysteresis model, *IEEE Trans. on Magnetics*, 49(5), 2405-2408, 2013.
 - [10] A. Darabi, M. Sadeghi, A. Hassannia, Design Optimization of Multistack Coreless Disk-Type Hysteresis Motor, *IEEE Trans. on Energy Conversion*, 26(4), 1081-1087, 2011.
 - [11] M. Jagiela, T. Garbiec, M. Kowol, Design of high-speed hybrid hysteresis motor rotor using finite element model and decision process, *IEEE Trans. on Magnetics*, 50(2), Article# 7021304, 2014.
 - [12] T Kubota, G. Watui and M. Itagati, Hysteresis motor using magnetically anisotropic Fe-Cr-CO magnet, *IEEE Trans on Magnetics*, 34(6), 3888-3896, 1998.
 - [13] L. I. Mendelsohn, Heat treating P6 alloy for special properties for a four element gyro system, *IEEE Trans on Magnetics*, Mag-9(3), 356-359, 1973.
 - [14] M. A. Rahman, A. M. Osheiba, T. A. Little, and G. R. Slemon, Effects of samarium cobalt permanent magnet on the performance of polyphase hysteresis-reluctance motors, *IEEE Trans. Magnetics.*, MAG-20(2), 1765-1767, 1984.
 - [15] G. Wakui and M. Itagaki, Magnetic hysteresis characteristics of the rotor ring for hysteresis motor, *Trans. IEE Jpn.*, 97-B(12), 794-801, 1977.
 - [16] G. Wakui, T. Kubota, and M. Itagaki, Experimental discussion for practical use of Fe-Cr-Co magnet hysteresis motor, *Trans. IEE Jpn.*, 106-B(1), 17-24, 1986.
 - [17] Genjiro Wakui, Kazumi Kurihara, Tomotsugu Kubota, Radial flux type hysteresis motor with rotor ring of copper-sprayed surface layer, *Electrical Engineering in Japan*, 112(4), 132-143, 1992.
 - [18] S. Miyari and T. Kataoka, A basic equivalent circuit of the hysteresis motor, *J. Inst. Elect. Eng. Japan*, 85(10), 1740-1748, 1965.
 - [19] T. Ishikawa and T. Kataoka, Basic Analysis of Disc-Type hysteresis motors, *J. Inst. Elect. Eng. Japan*, 101(6), 659-666, 1981.
 - [20] S. K. Hong, H. K. Kim, H. S. Kim and H. K. Jung, Torque Calculation of Hysteresis Motor Using Vector Hysteresis Model, *IEEE Trans. On Magnetics*, 36(4), 1932-1935, 2000.
 - [21] I.D. Mayergoz, Dynamic Preisach models of hysteresis, *IEEE Trans. on Magnetic*, 24(6), 2925-2927, 1988.
 - [22] M. A. Rahman, M. A. Copeland, and G. R. Slemon, An analysis of the hysteresis motor III-Parasitic losses, *IEEE Trans. Power App. Syst*, PAS-88, 954-960, 1969.
 - [23] G. Wakui and M. Tomita, Effect of harmonic flux density on the characteristics of hysteresis motor, *Trans. IEE Jpn.*, 102-B(1), 25-32, 1982.